

# Determining cooling rates from mica $^{40}\text{Ar}/^{39}\text{Ar}$ thermochronology data: effect of cooling path shape

C. S. McDonald<sup>1,2</sup>, C. J. Warren<sup>1\*</sup>, F. Hanke<sup>3</sup> and J. Chard<sup>4</sup>

<sup>1</sup>School of Environment, Earth and Ecosystem Sciences, The Open University, Walton Hall, Milton Keynes, MK7 6AA, United Kingdom

<sup>2</sup>School for Earth and Space Exploration, Arizona State University, BOX 876004, Tempe, Arizona, 85287-6004

<sup>3</sup>Dassault Systèmes, 334 Cambridge Science Park, Milton Road, Cambridge, CB4 0WN, United Kingdom

<sup>4</sup>School of Earth and Planetary Sciences, The Institute for Geoscience Research (TIGeR), Curtin University, Perth, WA 6845, Australia

\*clare.warren@open.ac.uk

*Keywords: Thermochronology, Diffusion Modelling, Closure Temperature, muscovite, biotite,  $^{40}\text{Ar}/^{39}\text{Ar}$*

## Abstract

Tectonic models are commonly underpinned by metamorphic cooling rates derived from diffusive-loss thermochronology data. Such cooling ages are usually linked to temperature via Dodson's 1973 closure temperature ( $T_C$ ) formulation, which specifies a 1/time-shaped cooling path. Geologists, however, commonly discuss cooling rates as a linear temperature/time shape. We present the results of a series of simple finite-difference diffusion models for Ar diffusion in muscovite and biotite that show that the difference in recorded age between 1/t and linear cooling paths increases significantly with hotter starting temperatures, slower cooling rates and smaller grain sizes. Our results show that it is essential to constrain the cooling path shape in order to make meaningful interpretations of the measured data.

## 35 Introduction

36 The ratio of parent to daughter radiogenic isotopes has been used for over a hundred  
 37 years to constrain geological ages and timescales (e.g. as reviewed by Condon and Schmitz,  
 38 2013). Minerals that host the radioactive parent element are commonly referred to as either  
 39 “geochronometers”, which record the timing of their crystallisation or  
 40 “thermochronometers”, which record the timing of cooling through an estimated temperature  
 41 window at some point after their crystallisation (e.g. as reviewed by Reiners, 2005). The  
 42 record of different time-temperature pairs in any one rock or tectonic region helps to  
 43 constrain thermal history and thus provide clues about the mechanism(s) by which the rocks  
 44 were exhumed to the surface.

45 Many thermochronometers are based on the premise that some of the daughter isotope  
 46 concentration is lost via thermally-activated diffusion at high temperatures, and that the  
 47 resulting mineral age can be linked to temperature via the mathematics governing such  
 48 diffusion. The temperature of a thermochronometer-bearing rock at the time the  
 49 thermochronometer recorded its apparent (bulk, whole-grain average) cooling age is most  
 50 commonly estimated using Dodson’s closure temperature ( $T_C$ ) formulation (Dodson 1973),  
 51 which, for thermally activated diffusion described by

$$52 \quad D = D_0 e^{-E_a/RT} \quad [1]$$

53 is given by:

$$54 \quad T_C = R/[E_a \ln(A\tau D_0/a^2)] \quad [2]$$

55 Where  $D$  is the diffusion coefficient,  $D_0$  is the diffusion pre-exponential factor,  $R$  is  
 56 the gas constant,  $E_a$  is the activation energy,  $a$  is the diffusion (or grain) radius,  $A$  is a grain-  
 57 shape-related constant and  $\tau$  relates the  $T_C$  to cooling rate:

$$58 \quad \tau = \frac{R}{(E_a dT^{-1}/dt)} = - \frac{RT^2}{(E_a dT/dt)} \quad [3]$$

59 This result of an analytical solution to the diffusion equation has had an enduring  
 60 legacy due to its mathematical elegance and simplicity of application. However the Dodson  
 61  $T_C$  formulation is underpinned by several important assumptions and approximations:

62 (1) that thermally activated volume diffusion was the only mechanism by which the  
 63 daughter isotope was mobilised within the mineral;

64 (2) that the mineral crystallized with no inherited daughter isotope;

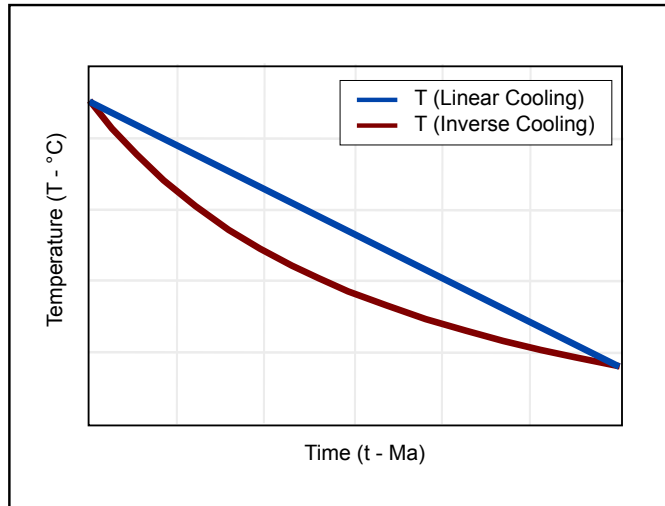
65 (3) that a daughter isotope concentration of zero was maintained at the mineral grain  
 66 boundary throughout cooling;

67 (4) that the starting temperature was high enough for diffusion of the daughter isotope  
 68 to be efficient, and removal from the grain to be geologically instantaneous, and

69 (5) that the cooling path from the time of crystallisation to the time of closure  
 70 conformed to a  $1/t$  (time) -shape.

71 These approximations have a major impact on the applicability of the formulation to  
 72 any particular geological scenario. The further any scenario deviates from these assumptions,  
 73 the greater the (commonly un-quantified and un-reported) interpretational uncertainties on the  
 74 link between age and temperature. A refinement of the  $T_C$  formulation to consider cases that  
 75 did not conform to point (4) was proposed by Ganguly and Tirone, 1999, but has not been  
 76 applied by the thermochronometer community to nearly the same extent that the original  
 77 Dodson formulation has been.

78 The Dodson closure temperature formulation is most commonly used to constrain  
 79 cooling rates by linking the  $T_C$  + time pair to a higher temperature + time pair linearly.  
 80 However,  $T_C$  has been derived explicitly for temperature histories that involve cooling  
 81 proportional to  $1/t$  (Figure 1) as this creates a linear time dependence in the exponent in  $\exp(-$   
 82  $E_a/RT)$  and allows the analytic integration of the time dependence. To calculate a closure  
 83 temperature using the Dodson  $T_C$  formulation and then to use that result to calculate a linear  
 84 cooling rate is therefore both circular (as also noted by e.g. Ganguly and Tirone, 2009) and  
 85 ultimately incorrect.



86

87 **Fig. 1.** A schematic representation showing the difference between linear (blue) and  
 88  $1/t$  (red) cooling paths. Note that the  $1/t$ -shaped path initially cools faster, therefore reducing  
 89 the opportunity for daughter product loss by diffusion.

90

91 Modern analytical equipment can now provide ever more precise isotope  
 92 concentration (age) data, at ever increasing spatial resolution. Furthermore, the diffusion  
 93 equation can be solved numerically on any standard computer. Here we investigate the

94 effects of linear and 1/t cooling path shapes on the bulk ages and core-rim age profiles of Ar  
95 in muscovite and biotite in grains of different radius that have cooled from different  
96 temperatures at different rates. The model results show that the ages recorded by muscovite  
97 and biotite that have cooled following these different simple end-member paths differ  
98 significantly, especially at higher peak temperatures increase and smaller grain sizes. The  
99 results also allow cooling rates to be determined directly if there is independent evidence for  
100 cooling path shape, so long as the time at which cooling started is known.

101

102

### 103 **The DiffArgP\_inverse Code**

104 The finite-difference code DiffArgP\_inverse is a modified version of DiffArg  
105 (Wheeler 1996). It is written in Matlab 4.1 and solves the diffusion equation numerically.  
106 DiffArgP\_inverse differs from DiffArg in that it includes the effect of pressure on the  
107 diffusion of Ar in muscovite (Harrison et al., 2009) and the functionality to model 1/t-shaped  
108 thermal histories to match the analytical solution of Dodson, 1973, rather than only linear or  
109 piecewise-linear histories. DiffArg and its modified variants has previously been used to  
110 model Ar diffusion in different minerals that experienced complex metamorphic histories in a  
111 variety of tectonic environments (e.g. Mark et al., 2008; Warren et al., 2012a;b; Wartho et al.,  
112 2013; McDonald et al., 2016; 2018). The code allows the user to input any thermal and  
113 (de)compression history and produces outputs of integrated single grain (bulk) ages and core-  
114 rim age profiles. Any of the DiffArg versions are available from Hanke or Warren on request.  
115 Further details of the DiffArg\_Inverse code are presented in Supplementary Document S1.

116

### 117 **Methods**

118 The bulk (volume-integrated)  $^{40}\text{Ar}/^{39}\text{Ar}$  ages of muscovite and biotite of different  
119 grain size were modelled for a variety of different starting temperatures and linear vs. inverse  
120 (1/t) cooling histories. Muscovite and biotite were modelled with cylindrical geometry and  
121 grain radii of 1 mm, 0.5 mm, and 0.25 mm as these are the most typical grain sizes picked for  
122 metamorphic  $^{40}\text{Ar}/^{39}\text{Ar}$  analyses. The diffusion parameters applied to each mineral are  
123 outlined in Table 1.

124 All minerals were modelled as “crystallising” then instantaneously cooling from  
125 starting temperatures of 700°C, 600°C, 500°C, and 450°C at a starting pressure of 1 GPa to  
126 represent a variety of metamorphic terranes exhuming from mid-crustal conditions (Tables 1,  
127 2, 4, Supplementary Tables S.2, S.4). A series of muscovite models was run at a starting  
128 pressure of 2 GPa to more closely match conditions found in subduction zones (c.f. Warren et

129 al., 2012a; Table 3, Supplementary Table S.3), and a further series of muscovite models was  
 130 run with spherical geometry to allow comparison with the cylindrical geometry models  
 131 (Supplementary Table S.5 and Figure S.6). Linear cooling rates of 5, 10, 25, 50, and 70°C/Ma<sup>-1</sup>  
 132 were run in order to compare results for typical rates of cooling in different tectonic terranes.  
 133 1/t cooling rate models were run for equivalent “time to reach 0°C” as the linear models, in  
 134 order to compare results for different cooling path shapes. Model pressures were decreased to  
 135 0 GPa over the same time interval.

136 The grain boundary conditions in all models were modelled as zero daughter element  
 137 concentration, for the purposes of investigating behaviour in an open system. Model ages  
 138 were calculated for 2-dimensional (cylindrical) diffusion geometry (Hames and Bowring  
 139 1994) and the time integration was performed using the Crank–Nicholson solver, with a  
 140 recommended time step that is 10 times larger than the value suggested for a stable fully-  
 141 explicit method (Table 1; Wheeler 1996).

142 A series of models was run to test the effect of the published experimental  
 143 uncertainties on  $E_a$  and  $D_0$  (Harrison et al., 2009 for muscovite and Harrison et al., 1985 for  
 144 biotite) on the model results. The results are detailed in Supplementary Table S.7.

145

146 **Table 1.** Diffusion and other model parameters used in this study.

147

<b>Modelled diffusion parameters</b>						
<b>Mineral</b>	<b>System</b>	<b><math>E_a</math></b> Jmol <sup>-1</sup>	<b><math>D_0</math></b> mm <sup>2</sup> s <sup>-1</sup>	<b><math>V_0</math></b> cm <sup>3</sup> mol <sup>-1</sup>	<b><math>P_0</math></b> Gpa	<b>Reference</b>
Muscovite	<sup>40</sup> Ar/ <sup>39</sup> Ar	263592	2.30E+02	14	1	Harrison et al., (2009)
Biotite	<sup>40</sup> Ar/ <sup>39</sup> Ar	196648	7.70E+00	0	0	Harrison et al., (1985)
<b>Other model parameters</b>						
<b>Mineral</b>	<b>System</b>	<b>Grain shape</b>	<b>Radius range</b> mm	<b>Starting temp range</b> °C	<b>Linear cooling rate range</b> °C/Ma	<b>Starting pressure range</b> GPa
Muscovite	<sup>40</sup> Ar/ <sup>39</sup> Ar	Cylinder	1-0.25	700-450	5, 10, 25, 50, 70	2-1
Biotite	<sup>40</sup> Ar/ <sup>39</sup> Ar	Cylinder	1-0.25	700-450	5, 10, 25, 50, 70	1
<b>Global model parameters</b>						

---

Grain boundary:	Zero concentration
Solver:	Crank-Nicholson
Time step	10

148

149

### **Results**

150

151

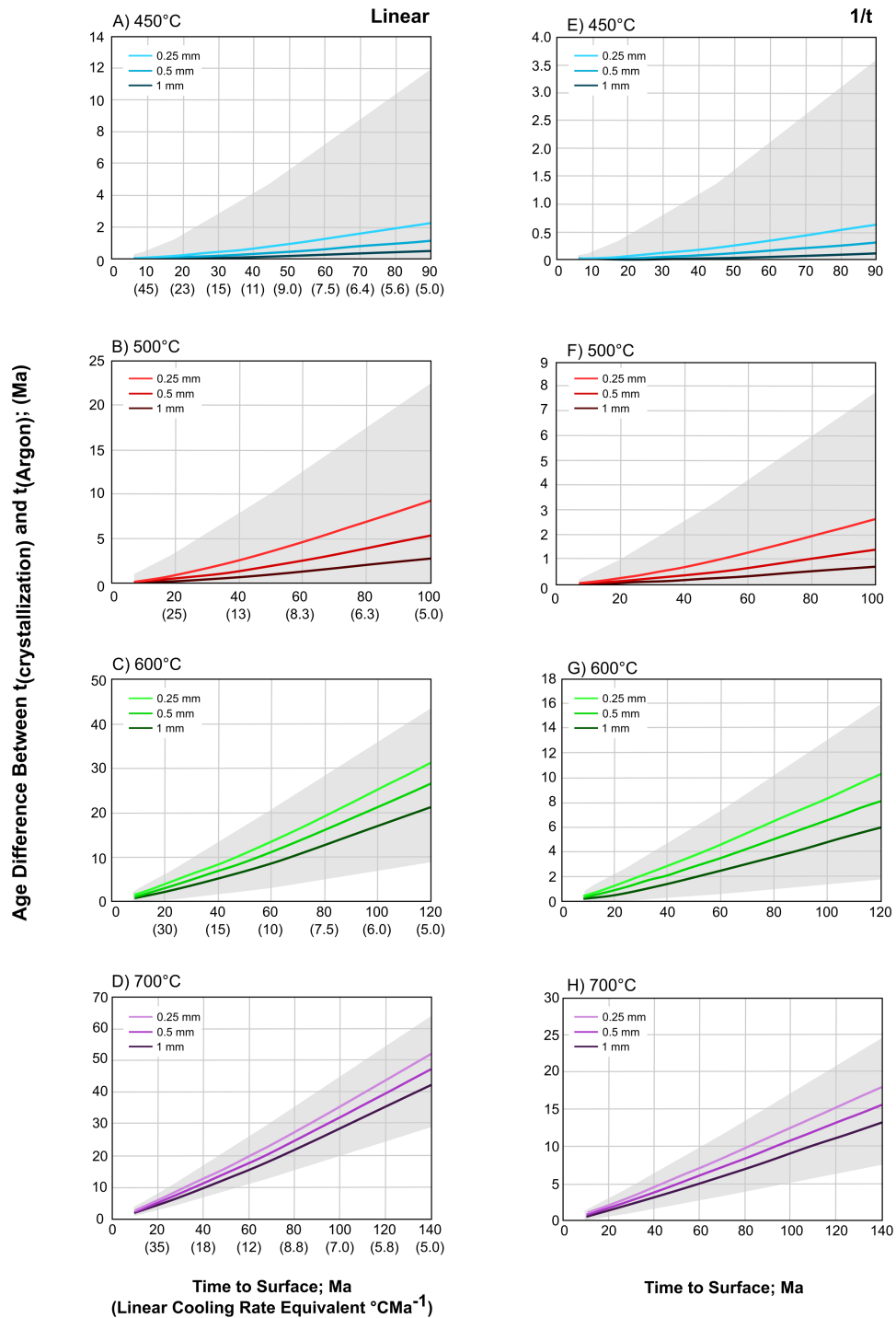
152

153

154

155

The model results are plotted in Figures 2 and 3 (Muscovite modelled from pressures of 1 GPa and 2 GPa respectively) and 4 (Biotite from 1 GPa). Summary model results for the bulk (volume-averaged) ages are presented in Tables 2 (Muscovite), and 3 (Biotite). Full results including core-rim model age variations are presented in Supplementary Tables S.2 (Muscovite 1 GPa) Table S.3 (Muscovite 2 GPa), Table S.4 (Biotite) and Table S.5 (Muscovite 1 GPa with spherical geometry).



156

157

158

159

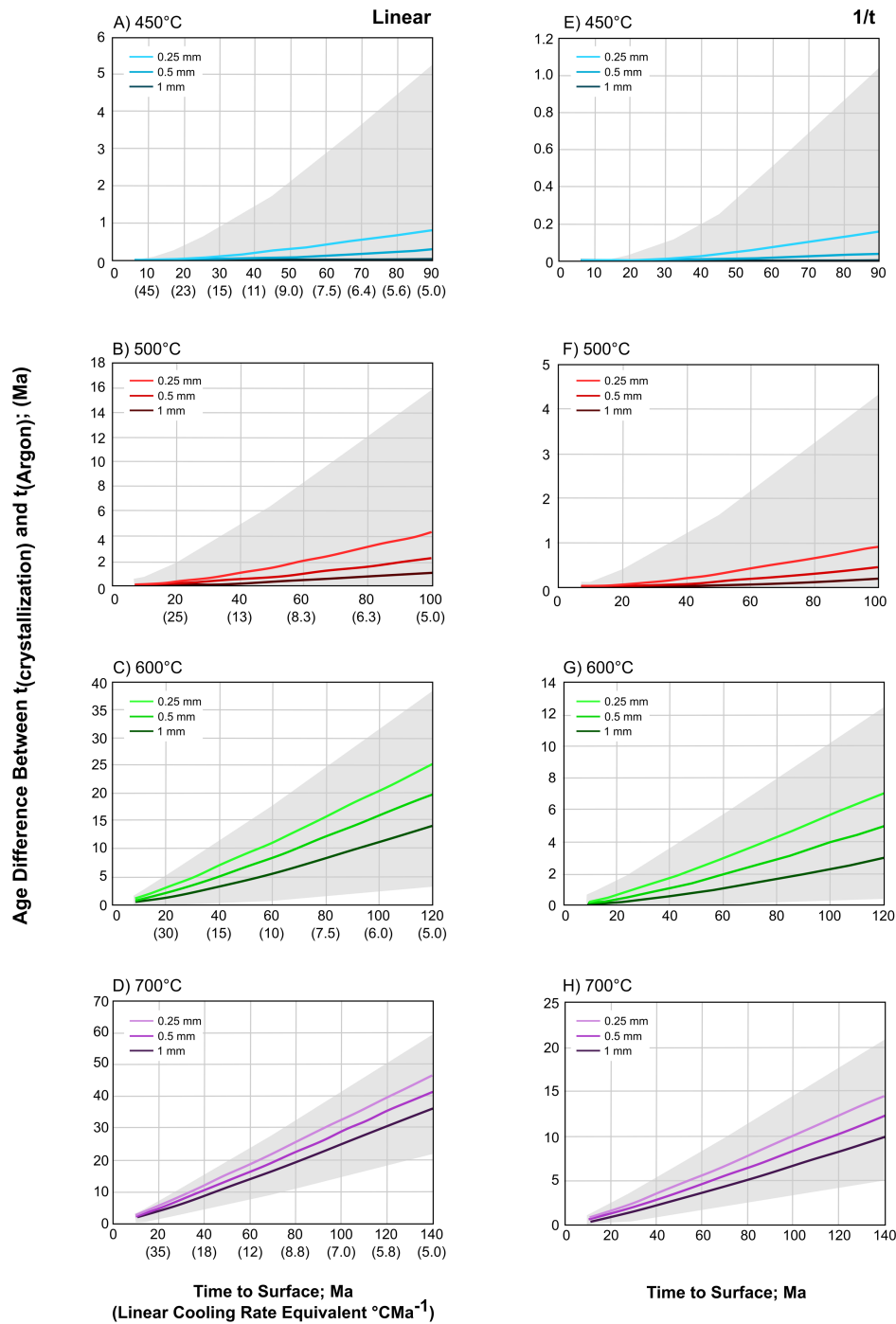
160

161

**Fig. 2.** Muscovite linear and 1/t results for models run at 1 GPa. Different coloured lines show different grain sizes. A-D show results for linear models at different starting temperatures; E-H show results for 1/t models that run over the same timescale. For ease of comparison, both sets of models run for the equivalent “time to surface” which is plotted on the x-axis. The equivalent linear rate is plotted underneath the “time to surface” value on

162 *the linear model plots. The y-axis plots the difference between the time at which cooling*  
163 *starts and the recorded  $^{40}\text{Ar}/^{39}\text{Ar}$  age: if this is, the grain size and the starting temperature*  
164 *are known for the analysed samples, then the cooling rate can be read off the graph directly.*  
165 *Note the differences in the y-axis scale between the linear and 1/t results. The grey outline*  
166 *maps the maximum uncertainty associated with the experimental diffusion parameters of*  
167 *Harrison et al., 2009 for the 0.5 mm grain-size models (the results for the other grain sizes*  
168 *will scale accordingly).*





169

170

171

172

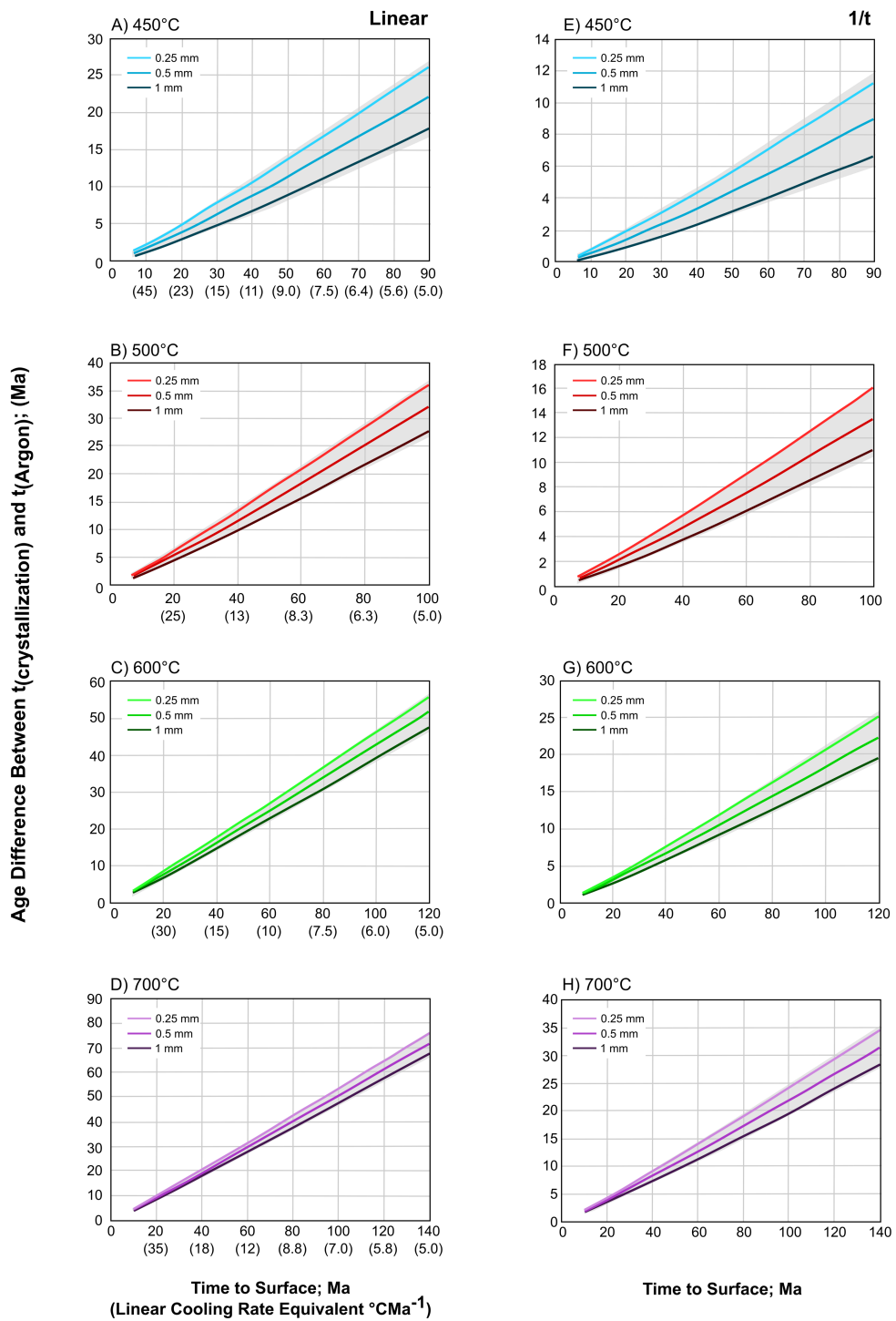
173

174

175

**Fig 3.** *Muscovite linear and 1/t results for models run at 2 GPa. Different coloured lines show different grain sizes. A-D show results for linear models at different starting temperatures; E-H show results for 1/t models that run over the same timescale. For ease of comparison, both sets of models run for the equivalent “time to surface” which is plotted on the x-axis. The equivalent linear rate is plotted underneath the “time to surface” value on the linear model plots. The y-axis plots the difference between the time at which cooling*

176 *starts and the recorded  $^{40}\text{Ar}/^{39}\text{Ar}$  age: if this is, the grain size and the starting temperature*  
177 *are known for the analysed samples, then the cooling rate can be read off the graph directly.*  
178 *Note the differences in the y-axis scale between the linear and 1/t results. The grey outline*  
179 *maps the maximum uncertainty associated with the experimental diffusion parameters of*  
180 *Harrison et al., 2009 for the 0.5 mm grain-size models (the results for the other grain sizes*  
181 *will scale accordingly).*  
182



183

184

185

186

187

188

**Fig. 4.** Biotite linear and 1/t model results. Different coloured lines show different grain sizes. A-D show results for linear models at different starting temperatures; E-H show results for 1/t models that run over the same timescale. For ease of comparison, both sets of models run for the equivalent “time to surface” which is plotted on the x-axis. The equivalent linear rate is plotted underneath the “time to surface” value on the linear model

189 plots. The y-axis plots the difference between the time at which cooling starts and the  
 190 recorded  $^{40}\text{Ar}/^{39}\text{Ar}$  age: if this is, the grain size and the starting temperature are known for  
 191 the analysed samples, then the cooling rate can be read off the graph directly. Note the  
 192 differences in the y-axis scale between the linear and  $1/t$  results. The grey outline maps the  
 193 maximum uncertainty associated with the experimental diffusion parameters of Harrison et  
 194 al., 2009 for the 0.5 mm grain-size models (the results for the other grain sizes will scale  
 195 accordingly).

196  
 197

198 **Table 2.** Model results for muscovite diffusion run with cylindrical geometry and at 1  
 199 GPa.

Linear Models		Cooling Rate ( $^{\circ}\text{C}\text{Ma}^{-1}$ )									
		5		10		25		50		70	
Grain Radius	T ( $^{\circ}\text{C}$ )	Time to $0^{\circ}\text{C}$ Ma	$\Delta t$ Ma	Time to $0^{\circ}\text{C}$ Ma	$\Delta t$ Ma	Time to $0^{\circ}\text{C}$ Ma	$\Delta t$ Ma	Time to $0^{\circ}\text{C}$ Ma	$\Delta t$ Ma	Time to $0^{\circ}\text{C}$ Ma	$\Delta t$ Ma
0.25 mm	450	90	2.40	45	0.84	18	0.20	9	0.07	6.4	0.04
	500	100	10.10	50	3.91	20	1.05	10	0.37	7.1	0.23
	600	120	31.26	60	14.45	24	5.13	12	2.31	8.6	1.58
	700	140	52.08	70	24.87	28	9.31	14	4.40	10	3.06
0.5 mm	450	90	1.15	45	0.38	18	0.09	9	0.03	6.4	0.01
	500	100	5.81	50	2.10	20	0.54	10	0.19	7.1	0.12
	600	120	26.45	60	11.96	24	4.10	12	1.78	8.6	1.18
	700	140	47.35	70	22.44	28	8.30	14	3.88	10	2.67
1 mm	450	90	0.52	45	0.16	18	0.03	9	0.01	6.4	0.00
	500	100	2.99	50	1.04	20	0.25	10	0.09	7.1	0.06
	600	120	21.33	60	9.31	24	2.99	12	1.21	8.6	0.76
	700	140	42.29	70	19.82	28	7.20	14	3.32	10	2.26

200

1/t Models		Cooling Rate ( $^{\circ}\text{C}\text{Ma}^{-1}$ )									
		5		10		25		50		70	
Grain Radius	T ( $^{\circ}\text{C}$ )	Time to $0^{\circ}\text{C}$ Ma	$\Delta t$ Ma	Time to $0^{\circ}\text{C}$ Ma	$\Delta t$ Ma	Time to $0^{\circ}\text{C}$ Ma	$\Delta t$ Ma	Time to $0^{\circ}\text{C}$ Ma	$\Delta t$ Ma	Time to $0^{\circ}\text{C}$ Ma	$\Delta t$ Ma
0.25 mm	450	90	0.58	45	0.19	18	0.05	9	0.02	6.4	0.01
	500	100	2.61	50	0.95	20	0.25	10	0.09	7.1	0.05
	600	120	10.27	60	4.60	24	1.56	12	0.67	8.6	0.44
	700	140	18.06	70	8.43	28	3.06	14	1.41	10	0.96
0.5 mm	450	90	0.26	45	0.08	18	0.02	9	0.00	6.4	0.00
	500	100	1.36	50	0.48	20	0.12	10	0.04	7.1	0.03

	600	120	8.12	60	3.52	24	1.13	12	0.46	8.6	0.29
	700	140	15.65	70	7.23	28	2.57	14	1.16	10	0.79
1 mm	450	90	0.10	45	0.03	18	0.00	9	0.00	6.4	0.00
	500	100	0.66	50	0.22	20	0.06	10	0.02	7.1	0.01
	600	120	5.97	60	2.45	24	0.70	12	0.26	8.6	0.16
	700	140	13.25	70	6.02	28	2.09	14	0.92	10	0.62

201

202

**Table 3.** Model results for muscovite diffusion run with cylindrical geometry and at 2

203

GPa.

Linear Models		Cooling Rate ( $^{\circ}\text{C}\text{Ma}^{-1}$ )									
		5		10		25		50		70	
Grain Radius	T ( $^{\circ}\text{C}$ )	Time to $0^{\circ}\text{C}$ Ma	$\Delta t$ Ma	Time to $0^{\circ}\text{C}$ Ma	$\Delta t$ Ma	Time to $0^{\circ}\text{C}$ Ma	$\Delta t$ Ma	Time to $0^{\circ}\text{C}$ Ma	$\Delta t$ Ma	Time to $0^{\circ}\text{C}$ Ma	$\Delta t$ Ma
0.25 mm	450	90	0.82	45	0.27	18	0.05	9	0.01	6.4	0.00
	500	100	4.33	50	1.56	20	0.40	10	0.14	7.1	0.09
	600	120	25.22	60	11.29	24	3.80	12	1.62	8.6	1.06
	700	140	47.06	70	22.27	28	8.21	14	3.83	10	2.63
0.5 mm	450	90	0.31	45	0.07	18	0.01	9	0.00	6.4	0.00
	500	100	2.24	50	0.80	20	0.20	10	0.07	7.1	0.04
	600	120	19.86	60	8.52	24	2.64	12	1.04	8.6	0.64
	700	140	41.87	70	19.58	28	7.08	14	3.25	10	2.21
1 mm	450	90	0.05	45	0.01	18	0.00	9	0.00	6.4	0.00
	500	100	1.12	50	0.38	20	0.08	10	0.02	7.1	0.01
	600	120	14.12	60	5.59	24	1.53	12	0.56	8.6	0.34
	700	140	36.32	70	16.69	28	5.87	14	2.62	10	1.76

204

1/t Models		Cooling Rate ( $^{\circ}\text{C}\text{Ma}^{-1}$ )									
Grain Radius	T ( $^{\circ}\text{C}$ )	Time to $0^{\circ}\text{C}$ Ma	$\Delta t$ Ma	Time to $0^{\circ}\text{C}$ Ma	$\Delta t$ Ma	Time to $0^{\circ}\text{C}$ Ma	$\Delta t$ Ma	Time to $0^{\circ}\text{C}$ Ma	$\Delta t$ Ma	Time to $0^{\circ}\text{C}$ Ma	$\Delta t$ Ma
0.25 mm	450	90	0.16	45	0.04	18	0.01	9	0.00	6.4	0.00
	500	100	0.94	50	0.33	20	0.08	10	0.03	7.1	0.02
	600	120	7.11	60	3.03	24	0.93	12	0.37	8.6	0.23
	700	140	14.68	70	6.75	28	2.39	14	1.07	10	0.73
0.5 mm	450	90	0.04	45	0.01	18	0.00	9	0.00	6.4	0.00
	500	100	0.47	50	0.16	20	0.04	10	0.01	7.1	0.00
	600	120	5.01	60	1.99	24	0.54	12	0.20	8.6	0.12
	700	140	12.32	70	5.58	28	1.92	14	0.84	10	0.56
1 mm	450	90	0.00	45	0.00	18	0.00	9	0.00	6.4	0.00
	500	100	0.21	50	0.06	20	0.01	10	0.00	7.1	0.00

600	120	3.01	60	1.10	24	0.28	12	0.10	8.6	0.06
700	140	9.98	70	4.41	28	1.46	14	0.61	10	0.40

205

206

207

**Table 4. Model results for biotite diffusion.**

Cooling Rate ( $^{\circ}\text{C}\text{Ma}^{-1}$ )

Linear Models		5		10		25		50		70	
Grain Radius	Starting T ( $^{\circ}\text{C}$ )	Time to $0^{\circ}\text{C}$ Ma	$\Delta t$ Ma	Time to $0^{\circ}\text{C}$ Ma	$\Delta t$ Ma	Time to $0^{\circ}\text{C}$ Ma	$\Delta t$ Ma	Time to $0^{\circ}\text{C}$ Ma	$\Delta t$ Ma	Time to $0^{\circ}\text{C}$ Ma	$\Delta t$ Ma
0.25 mm	450	90	25.88	45	11.89	18	4.24	9	1.91	6.4	1.27
	500	100	35.88	50	16.92	20	6.24	10	2.91	7.1	2.00
	600	120	55.88	60	26.92	24	10.24	12	4.91	8.6	3.41
	700	140	75.88	70	36.92	28	14.24	14	6.91	10	4.87
0.5 mm	450	90	21.82	45	9.78	18	3.34	9	1.42	6.4	0.96
	500	100	31.82	50	14.82	20	5.34	10	2.49	7.1	1.63
	600	120	51.82	60	24.82	24	9.34	12	4.49	8.6	3.11
	700	140	71.82	70	34.82	28	13.34	14	6.49	10	4.56
1 mm	450	90	17.45	45	7.54	18	2.39	9	0.96	6.4	0.63
	500	100	27.45	50	12.51	20	4.39	10	1.97	7.1	1.28
	600	120	47.45	60	22.51	24	8.39	12	3.97	8.6	2.77
	700	140	67.45	70	32.51	28	12.39	14	5.97	10	4.21

208

1/t Models		5		10		25		50		70	
Grain Radius	T ( $^{\circ}\text{C}$ )	Time to $0^{\circ}\text{C}$ Ma	$\Delta t$ Ma	Time to $0^{\circ}\text{C}$ Ma	$\Delta t$ Ma	Time to $0^{\circ}\text{C}$ Ma	$\Delta t$ Ma	Time to $0^{\circ}\text{C}$ Ma	$\Delta t$ Ma	Time to $0^{\circ}\text{C}$ Ma	$\Delta t$ Ma
0.25 mm	450	90	11.10	45	4.97	18	1.67	9	0.75	6.4	0.49
	500	100	15.76	50	7.25	20	2.62	10	1.18	7.1	0.80
	600	120	25.13	60	11.85	24	4.42	12	2.08	8.6	1.42
	700	140	34.39	70	16.45	28	6.23	14	2.95	10	2.07
0.5 mm	450	90	8.77	45	3.83	18	1.19	9	0.52	6.4	0.33
	500	100	13.31	50	6.03	20	2.14	10	0.94	7.1	0.63
	600	120	22.31	60	10.45	24	3.83	12	1.76	8.6	1.23
	700	140	31.40	70	14.89	28	5.54	14	2.65	10	1.80
1 mm	450	90	6.45	45	2.64	18	0.79	9	0.31	6.4	0.19
	500	100	10.81	50	4.76	20	1.58	10	0.69	7.1	0.45
	600	120	19.54	60	9.06	24	3.24	12	1.47	8.6	1.04
	700	140	28.28	70	13.33	28	4.93	14	2.36	10	1.58

209

210 The graphs all show similar trends:

211 (1) Faster cooling results in a smaller difference in time between the timing of  
212 maximum temperature attainment (cooling initiation) and the recorded cooling age ( $\Delta t$ ).

213 (2) Colder initial “peak” starting temperatures result in smaller  $\Delta t$ .

214 (3) Smaller grain sizes result in larger  $\Delta t$ .

215 (4) Smaller  $\Delta t$  values are recorded for the  $1/t$  models than for the linear models.

216 Results (1) and (3) are consistency checks to show that the models are behaving as  
217 expected. Result (2) similarly matches the predictions of the modified formulation of  
218 Ganguly and Tirone, 1999. Result (4) clearly shows the importance of the cooling path shape  
219 on the resulting thermochronometer age – this will be discussed further below.

220 Figure 2 shows that very little diffusive loss is expected in white mica grains that cool  
221 from relatively low peak temperatures of 450°C. The  $^{40}\text{Ar}/^{39}\text{Ar}$  age of a 0.25 mm radius white  
222 mica grain cooling linearly at a rate of 5°C $\text{Ma}^{-1}$  from 450°C and 1 GPa would be expected to  
223 be 2.4 Ma younger than the peak temperature age, whereas one cooling from 700°C would be  
224 expected to yield an age that is 52 Ma younger (Table 2). Similarly, the  $^{40}\text{Ar}/^{39}\text{Ar}$  age of a  
225 0.25 mm radius white mica grain cooling linearly at a rate of 5°C $\text{Ma}^{-1}$  from 600°C and 2 GPa  
226 would be expected to be ~25 Ma younger than the peak temperature age (Table 3). Similar-  
227 sized grains cooling to 0°C over the same time interval but following a  $1/t$  path from 450°C  
228 or 700°C at 1 GPa would only yield ages that were 0.6 or 16 Ma younger than the peak  
229 temperature age. A 1 mm radius grain cooling from 450°C, however, would be expected to  
230 record an age within uncertainty of the timing of peak metamorphism.

231 Models run using spherical diffusion geometry yield slightly younger ages ( $\Delta t$  of 54  
232 Ma rather than 52 Ma for a 0.25 mm radius grain cooling from 700°C at 5°C $\text{Ma}^{-1}$  for  
233 example; Supplementary Table S.5; Supplementary Figure S.6).

234 Figure 3 shows that biotite should yield significantly younger ages than muscovite for  
235 grains of the same radius, cooling from the same starting temperature and following the same  
236 cooling path. For example a 0.25 mm radius grain cooling at 5°C $\text{Ma}^{-1}$  from 450°C would be  
237 expected to be 26 Ma younger than the age of peak temperature metamorphism, whereas one  
238 cooling from 700°C at the same rate would be expected to yield an age that was 76 Ma  
239 younger (Table 3).

240

## 241 Discussion

242 The results clearly show that the shape of the cooling path makes an increasingly  
243 important contribution to the recorded thermochronometer age as grain sizes and cooling

244 rates decrease and peak temperatures increase. The uncertainty inherent in using the Dodson  
245  $T_C$  formulation to estimate (linear) cooling rates therefore also magnifies accordingly.

246 The model results are more sensitive to systematic uncertainties in the  
247 experimentally-determined activation energy ( $E_a$ ) than in the exponential pre-factor ( $D_0$ ) for  
248 each mineral (Figures 2-4 and Supplementary Table S.7). These figures show that  
249 uncertainties in the diffusion parameters have a significant, but systematic, effect on the  
250 recorded thermochronological ages. These uncertainties apply equally to both cooling history  
251 shapes discussed here.

252 The most recent diffusion parameters for muscovite (Harrison et al., 2009) were  
253 calculated for isotropic 3-dimensional (spherical) diffusion geometry. It has been suggested  
254 that modelling muscovite as a cylinder but using diffusion parameters calculated for spherical  
255 geometry invalidates the results (Foster and Lister, 2017). However the overall difference in  
256 the diffusion coefficient is a factor 2 in  $D_0$ , which translates into an activation barrier of  $<0.6$   
257 kcal/mol at 400 K. This is well below the uncertainty of 7 kcal/mol in the Harrison et al.,  
258 2009 diffusion parameters and thus adds no extra uncertainty to our overall results, as also  
259 suggested in other studies (e.g. Huber et al., 2011).

260

### 261 **Applying Model Results to Natural Systems**

262 The results presented here can be used to constrain the cooling rates of natural  
263 systems if the following pieces of information are known or can be estimated:

264 1) A petrographically-based interpretation of the temperature at which the dated  
265 grain(s) grew, and the portion of the metamorphic path along which the grain(s) grew (e.g.  
266 prograde peak or retrograde). This will inform and constrain the extent of diffusive  
267 opportunity that the grain could have experienced. For example a grain growing during the  
268 prograde history will have longer residence at high temperatures, therefore allowing it more  
269 opportunity to lose argon.

270 2) The peak temperature experienced by the grain(s), required for the ultimate  
271 determination of a cooling rate.

272 3) The time at which the grain reached its peak temperature (constrained or estimated  
273 by independent geochronometers), required for the ultimate determination of a cooling rate.  
274 This is further discussed below.

275 4) The thermochronometric ages of the grains of interest; different data collection  
276 methods are further discussed below.

277 5) The grain size(s) of the dated grains.



278           6) The assumption or knowledge that open grain-boundary, thermally-activated  
279 diffusion was the dominant process in determining the final Ar concentration. This  
280 approximation is difficult to assess (e.g. Warren et al., 2012a,b) but should be acknowledged  
281 in any thermochronological interpretation.

282           Note that only very simple cooling path shapes have been modelled here. Steady  
283 progress is being made in the development of modelling tools that can suggest a “best fit”  
284 cooling path to U-Th-He, fission track and U-Pb rutile data, but currently none of these tools  
285 explicitly incorporate  $^{40}\text{Ar}/^{39}\text{Ar}$  data: e.g. HeFTy (Ketcham, 2005), QTQt (Gallagher, 2012),  
286 UpBeat (Smye et al., 2018).

287

288           **Determining the timing of cooling initiation:** Direct determination of a cooling rate  
289 (and cooling rate shape) from thermo- and geochronological data requires that at least two,  
290 and possibly three, T-t pairs are known. Timing of peak T in metamorphic rocks is  
291 commonly constrained by U-Pb ages of zircon, monazite, garnet, allanite and/or rutile, with  
292 secondary (higher-temperature cooling) T-t pairs provided by U-Pb rutile and/or titanite data.  
293 There are, of course, multiple uncertainties inherent in linking these ages to peak temperature  
294 because all of these minerals may crystallise at different stages of the metamorphic PT path.  
295 Careful petrochronological investigation is required to confirm that the ages yielded by any  
296 of these minerals relate to the timing of attainment of peak temperatures or higher-than-  
297 argon-closure cooling (e.g. Kohn et al., 2017).

298

299            **$^{40}\text{Ar}/^{39}\text{Ar}$  data collection methods:**  $^{40}\text{Ar}/^{39}\text{Ar}$  mica data can currently be collected in  
300 many different ways: by multiple- or single-grain step heating experiments (e.g. Turner,  
301 1970), by single grain fusion methods (e.g. Fleck and Carr, 1990) or by laser ablation (e.g.  
302 Kelley et al., 1994). All methods have their advantages and disadvantages in terms of volume  
303 of material analysed, analytical precision and petrographic (location) control on age.

304           The model data presented here are compatible for assessment against the bulk  
305 (volume-averaged) ages – i.e. equivalent to single grain fusion  $^{40}\text{Ar}/^{39}\text{Ar}$  data. We caution  
306 against using multiple-or single-grain step heating  $^{40}\text{Ar}/^{39}\text{Ar}$  ages to compare against model  
307 results. Plateau ages imply no core-rim variation in Ar distribution, (and thus an  
308 interpretation of rapid cooling), but a plateau result does not in itself guarantee that the  
309 calculated age is geologically meaningful, especially in high pressure metamorphic rocks  
310 (e.g. Sherlock and Arnaud, 1999). Non-plateau spectra can be produced by a variety of  
311 factors that complicate linking spectrum shapes to within-grain Ar distribution. Single grain

312 fusion populations can help provide an assessment of how homogeneous Ar is distributed  
313 across mica grains within individual samples (e.g. Uunk et al., 2018).

314 In-situ, high-spatial precision  $^{40}\text{Ar}/^{39}\text{Ar}$  data such as collected by laser ablation  
315 methods, and collected in grains large enough and cooled slowly enough from a high enough  
316 temperature to be able to detect such changes, can also be assessed against the core-rim  
317 model age predictions for simple linear and  $1/t$  cooling histories presented in Supplementary  
318 Tables S.2 -S.4.

319

320 **Comparing analytical data to model results:** The time difference ( $\Delta t$ ) between the  
321 timing of the thermal peak (or to be absolutely correct, the timing of cooling initiation) and  
322 the age recorded by the thermochronometer (Figures 2-4 ) provides a basis for determining  
323 cooling rates under the fundamental approximations (1) that thermally activated volume  
324 diffusion was the only mechanism by which the daughter isotope was mobilised within the  
325 mineral; (2) that the mineral crystallized with no inherited daughter isotope; and (3) that the  
326 experimentally-derived diffusion parameters mimic what happens in nature. It is important to  
327 acknowledge that minerals may not degas in a high-vacuum environment in an experiment  
328 that lasts a few days in the same way that a mineral degasses in a rock over millions of years,  
329 however these experimental data are the best available at the present day.

330 For example, consider a scenario whereby a 0.5 mm radius muscovite in a rock that  
331 started cooling from 500°C at 100 Ma yields an age of 94 Ma.  $\Delta t$  is therefore 6 Ma. Table 2  
332 and Figure 2 suggest that those data are compatible with a linear cooling rate of 5°C/Ma<sup>-1</sup>.  
333 However this is not enough information to determine whether (a) the system was diffusively  
334 open (a fundamental requirement of any diffusive-based interpretative link between age,  
335 temperature and cooling rate is that effectively there is infinite sink for the daughter element  
336 diffusing out of the mineral grain) and/or (b) whether the cooling path was overall linear or  
337 some other shape. Both of these can be resolved following a match between data and model  
338 predictions.

339 For example, a rock cooling from 600°C might yield 1 mm radius biotite grains with a  
340  $\Delta t$  of 9 Ma, 0.5 mm radius grains with a  $\Delta t$  of 10.5 Ma and 0.25 mm radius grains with a  $\Delta t$   
341 of 12 Ma. These data would be compatible with a cooling path of  $1/t$  shape that cooled to  
342 0°C over 60 Ma. A minimum of two different ages – either different grain sizes of the same  
343 mineral or different minerals, should allow differentiation of the best-fit cooling path.

344 At rapid cooling rates, the difference between the cooling ages predicted by a linear  
345 temperature decrease and a  $1/t$ -shaped path would be indistinguishable within the typical  
346 uncertainties in analytical results and in the experimental diffusion parameters. At cooling

347 rates  $<10^{\circ}\text{C}\text{Ma}^{-1}$ , differences in the shapes of the cooling paths start to become important for  
348 distinguishing between exhumation mechanisms.

349 Small values of  $\Delta t$  e.g.  $< 1$  Ma are currently challenging to resolve analytically. The  
350 mica  $^{40}\text{Ar}/^{39}\text{Ar}$  models for low starting temperatures confirm previous suggestions that  
351 rapidly-cooled rocks that reached low peak temperatures (such as in subduction zones) will  
352 not yield ages that allow cooling rates to be determined.

353

354 **Other factors affecting daughter element distribution:** Inheritance or loss of  
355 daughter product during recrystallization and deformation during cooling can affect daughter  
356 element concentrations much more than diffusion (Villa 1998; Allaz et al., 2011; Villa et al.,  
357 2014). It is also obvious that re-crystallisation during exhumation means that the temperature  
358 that that particular grain cooled from may be lower than the peak temperature. In cases where  
359 thermochronometer minerals show signs of secondary recrystallization or other chemical  
360 modification, the model results are almost certainly not applicable, and a link between  
361 temperature and age may be more difficult to constrain. The diffusion models are *only*  
362 applicable to rocks in which an open system can be assumed, and where both the timing and  
363 pressure-temperature conditions of the last episode of mineral crystallisation are known or  
364 can be estimated.

365 If the results presented here are used to estimate cooling rates or constrain cooling  
366 path shapes, each practitioner will need to estimate the geological uncertainty for their  
367 particular study, noting that this is almost certainly the largest overall source of error in their  
368 interpretation. Our results are based on the assumption that cooling starts directly after the  
369 model grain has crystallised at peak temperatures. In reality, the minerals of interest may  
370 have grown along the prograde path and/or have resided at peak temperatures for a  
371 geologically-significant period of time before cooling started. If temperatures were low  
372 enough for diffusion to be inefficient, some of that pre-cooling history may be recorded in the  
373 thermochronometer minerals. Thermochronologists should model the effect of pre-peak  
374 thermal history for their particular geological location to convince themselves whether or not  
375 the thermochronometer minerals in their study area may record this.

376

### 377 **Conclusions**

378 The rates and timescales over which rocks are buried, transformed, deformed and  
379 exhumed help constrain the tectonic mechanisms that act on them.  $^{40}\text{Ar}/^{39}\text{Ar}$  data from micas  
380 have long been used to link time to temperature and thus constrain cooling rates. The  
381 Dodson closure temperature formulation (Dodson, 1973) provides an elegant analytical

382 solution to the diffusion equation but its application for determining cooling rates is  
383 commonly based on assumptions that are a poor match to geological reality. Our results of a  
384 series of diffusion models that quantify the differences in age expected from a simple linear  
385 and 1/t-shaped cooling histories show that the cooling path shape exerts considerable  
386 influence on the resulting age at hotter starting temperatures, slower cooling rates and smaller  
387 grain sizes. If the cooling path shape and timing of cooling initiation are known, then our  
388 results also provide a simple way of estimating cooling rates and cooling rate shapes from the  
389 difference between the timing of cooling initiation at maximum temperature and the yielded  
390 thermochronometer age. Future incorporation of  $^{40}\text{Ar}/^{39}\text{Ar}$  diffusion systematics into forward  
391 modelling packages that also incorporate other thermochronometers provides the best future  
392 solution for constraining cooling rates, with the caveat that more precise diffusion data are  
393 needed.

394

395

#### 396 **Acknowledgements**

397 CSM was funded on an Open University Charter Studentship. CJW acknowledges prior  
398 financial support from a NERC Advanced Fellowship (NE/H016279/1) and a NERC small  
399 grant (NE/J013072/1). The authors thank Simon Kelley for many fruitful discussions about  
400 linking age to stage and open system behaviour, and Leo Ingvorsen for helping to run some  
401 of the early models. CSM thanks Sarah Sherlock and Alison Halton for PhD supervision and  
402 guidance.

403

404

405

#### 406 **References**

407 Allaz, J., Engi, M., Berger, A. & Villa, I. 2011. The Effects of Retrograde Reactions and of  
408 Diffusion on  $^{40}\text{Ar}/^{39}\text{Ar}$  Ages of Micas. *Journal of Petrology*, 52, 691–716, doi:  
409 10.1093/petrology/egq100.

410 Condon, D. J. & Schmitz, M. D. One hundred years of isotope geochronology, and counting.  
411 *Element*, 9, 15-17, doi: 10.2113/gselements.9.1.15.

412 Dodson, M. H. 1973. Closure temperatures in cooling geological and petrological systems.  
413 *Contrib. Mineral. Petrol.*, 40, 259–274, doi: 10.1007/BF00373790.

414 Fleck, R.J. and Carr, M.D., 1990. The age of the Keystone Thrust: Laser-fusion  $^{40}\text{Ar}/^{39}\text{Ar}$   
415 dating of Foreland Basin Deposits, southern Spring Mountains, Nevada. *Tectonics*, 9,  
416 467-476.

- 417 Forster, M. A. & Lister, G. S. 2017,  $^{40}\text{Ar}/^{39}\text{Ar}$  geochronology and the diffusion of  $^{39}\text{Ar}$  in  
418 phengite-muscovite intergrowths during step-heating experiments in vacuo. In  
419 Jourdan, F., Mark, D. F. & Verati, C. (eds) 2014. *Advances in  $^{40}\text{Ar}/^{39}\text{Ar}$  Dating: from*  
420 *Archaeology to Planetary Sciences*. Geological Society, London, Special Publications,  
421 378, 117–135, doi: 10.1144/SP378.16.
- 422 Gallagher, K., 2012. Transdimensional inverse thermal history modeling for quantitative  
423 thermochronology. *J. Geophys. Res. Solid Earth*, 117, doi: 10.1029/2011JB008825
- 424 Ganguly J, Tirone M. 1999. Diffusion closure temperature and age of a mineral with arbitrary  
425 extent of diffusion: theoretical formulation and applications. *Earth and Planetary*  
426 *Science Letters*, 170, 131-40.
- 427 Ganguly J, Tirone M. 2009. Closure temperature, cooling age and high temperature  
428 thermochronology. In: *Physics and Chemistry of the Earth's Interior* (pp. 89-99).  
429 Springer, New York, NY.
- 430 Hames, W. E. & Bowring, S. A. 1994. An empirical evaluation of the argon diffusion  
431 geometry in muscovite. *Earth and Planetary Science Letters*, 124, 161–167,  
432 doi:10.1016/0012-821X(94)00079-4.
- 433 Harrison, T. M., Duncan, I. & McDougall, I. 1985. Diffusion of  $^{40}\text{Ar}$  in biotite: Temperature,  
434 pressure and compositional effects. *Geochimica et Cosmochimica Acta*, 49, 2461-  
435 2468, doi: 10.1016/0016-7037(85)90246-7.
- 436 Harrison, T. M., Celerier, J., Aikman, A. B., Hermann, J. & Heizler, M. T. 2009. Diffusion of  
437  $^{40}\text{Ar}$  in muscovite. *Geochim. Cosmochim. Acta.*, 73, 1039-1051, doi:  
438 10.1016/j.gca.2008.09.038.
- 439 Huber, C., Cassata, W.S. & Renne, P.R. 2011. A lattice Boltzmann model for noble gas  
440 diffusion in solids: The importance of domain shape and diffusive anisotropy and  
441 implications for thermochronometry. *Geochim. Cosmochim. Acta.*, 8, 2170-2186.  
442 doi:10.1016/j.gca.2011.01.039.
- 443 Kelley, S. P., Arnaud, N. O., and Turner, S. P., 1994. High spatial resolution  $^{40}\text{Ar}/^{39}\text{Ar}$   
444 investigations using an ultra-violet laser probe extraction technique. *Geochim.*  
445 *Cosmochim. Acta.*, 58, 3519-3525.
- 446 Ketchum, R.A., 2005. Forward and inverse modeling of low-temperature thermochronometry  
447 data. *Rev. Mineral. Geochem.*, 58, 275-314.
- 448 Kohn, M.J., Engi, M., Lanari, P. (eds), 2017. *Petrochronology: Methods and Applications*.  
449 *Reviews in Mineralogy* 83, pp 575. ISBN 978-0-939950-05-8
- 450 Mark, D. M., Kelley, S. P., Lee, M. R., Parnell, J., Sherlock, S. C. & Brown, D. J., 2008. Ar-  
451 Ar dating of authigenic K-feldspar: Quantitative modelling of radiogenic argon-loss

- 452 through subgrain boundary networks. *Geochimica et Cosmochimica Acta*, 72, 2695-  
453 27100, doi: 10.1016/j.gca.2008.03.018.
- 454 McDonald, C. S., Warren, C. J., Mark, D. F., Halton, A. M., Kelley, S. P. & Sherlock, S. C.,  
455 2016. Ar redistribution during a metamorphic cycle: Consequences for determining  
456 cooling rates. *Chemical Geology*, 443, 182-197, doi: 10.1016/j.chemgeo.2016.09.028.
- 457 Reiners, P. W., 2005. Past, Present, and Future of Thermochronology. *Reviews in*  
458 *Mineralogy and Geochemistry*. 58: 1. doi:10.2138/rmg.2005.58.1
- 459 Sherlock, S.C. and Arnaud, N.O., 1999. Flat plateau and impossible isochrons: Apparent  
460  $^{40}\text{Ar}$ - $^{39}\text{Ar}$  geochronology in a high-pressure terrain. *Geochimica et Cosmochimica*  
461 *Acta*, 63, 2835-2838.
- 462 Smye, A.J., Marsh, J.H., Vermeesch, P., Garber, J.M., Stockli, D.F., 2018. Applications and  
463 limitations of U-Pb thermochronology to middle and lower crustal thermal histories.  
464 *Chemical Geology* 494, 1-18. doi: 10.1016/j.chemgeo.2018.07.003
- 465 Turner, G., 1970.  $^{40}\text{Ar}/^{39}\text{Ar}$  age determination of lunar rock 12013. *Earth and Planetary*  
466 *Science Letters*, 9, 177-180.
- 467 Uunk B, Brouwer F, ter Voorde M, Wijbrans J., 2018. Understanding phengite argon closure  
468 using single grain fusion age distributions in the Cycladic Blueschist Unit on Syros,  
469 Greece. *Earth and Planetary Science Letters*, 484, 192-203.
- 470 Villa, I. M., 1998. Isotopic Closure. *Terra Nova*, 10, 42-47, doi: 10.1046/j.1365-  
471 3121.1998.00156.x
- 472 Villa, I. M., Bucher, S., Bousquet, R., Kleinhanns, I. C. & Schmid, S. M., 2014. Dating  
473 polygenetic metamorphic assemblages along a transect across the western Alps.  
474 *Journal of Petrology*, 55, 803–830, doi: 10.1093/petrology/egu007.
- 475 Warren, C. J., Hanke, F. & Kelley, S. P. 2012a. When can muscovite  $^{40}\text{Ar}/^{39}\text{Ar}$  dating  
476 constrain the timing of metamorphic exhumation? *Chemical Geology*, 291, 79–86,  
477 doi: 10.1016/j.chemgeo.2011.09.017.
- 478 Warren, C. J., Kelley, S. P., Sherlock, S. C. & McDonald, C. S. 2012b. Metamorphic rocks  
479 seek meaningful cooling rate: Interpreting  $^{40}\text{Ar}/^{39}\text{Ar}$  ages in an exhumed ultra-high  
480 pressure terrane. *Lithos*, 155, 30-48, doi: 10.1016/j.lithos.2012.08.011.
- 481 Wartho, J.-A., Kelley, S. P. & Elphick, S. C. 2013. Ar diffusion and solubility measurements  
482 in plagioclase using ultra-violet laser depth-profiling techniques. *Geological Society*,  
483 *London, Special Publications*, 378, 137-154, doi: 10.1144/SP378.13.
- 484 Wheeler, J. 1996. DIFFARG: A program for simulating argon diffusion profiles in minerals.  
485 *Computers and Geosciences*, 22, 919–929, doi: 10.1016/S0098-3004(96)00061-1.
- 486

487  
488  
489  
490  
491  
492  
493  
494  
495  
496  
497  
498  
499  
500  
501  
502  
503  
504  
505  
506  
507  
508  
509  
510  
511  
512  
513  
514  
515

## **Supplementary Data**

### **S.1 Instructions for operating DiffargP\_inverse**

### **S.2 Full muscovite results for 1GPa models**

### **S.3 Full muscovite results for 2GPa models**

### **S.4 Full biotite model results**

### **S.5. Full muscovite results for spherical geometry models**

**S.6. Muscovite linear and 1/t results for models run at 1 GPa with spherical geometry.** Different coloured lines show different grain sizes. A-D show results for linear models at different starting temperatures; E-H show results for 1/t models that run over the same timescale. For ease of comparison, both sets of models run for the equivalent “time to surface” which is plotted on the *x*-axis. The equivalent linear rate is plotted underneath the “time to surface” value on the linear model plots. The *y*-axis plots the difference between the time at which cooling starts and the recorded  $^{40}\text{Ar}/^{39}\text{Ar}$  age: if this is, the grain size and the starting temperature are known for the analysed samples, then the cooling rate can be read off the graph directly. Note the differences in the *y*-axis scale between the linear and 1/t results.

### **S.7. Results of sensitivity tests**